

## The cluster of galaxies A 2163B at $z \sim 0.2$

### I – Photometric properties. ★

F. La Barbera<sup>1</sup>, M. Massarotti<sup>1</sup>, P. Merluzzi<sup>1</sup>, G. Busarello<sup>1</sup>, and A. Mercurio<sup>2</sup>

<sup>1</sup> I.N.A.F., Istituto Nazionale di Astrofisica Osservatorio Astronomico di Capodimonte, Via  
Moiariello 16, I-80131 Napoli

email: labarber@na.astro.it

<sup>2</sup> Università degli Studi di Trieste, Department of Astronomy, Trieste

Received ; accepted

**Abstract.** We have performed a comprehensive photometric study of the galaxy population in the field of A 2163B, an extended X-ray source near the cluster of galaxies A 2163 at redshift  $z = 0.201$ . In the first paper, we present the photometric BVR<sub>I</sub>K data-set and discuss the integrated photometric properties for the galaxies in the field of A 2163B. The optical–NIR colour-magnitude relations and the K-band luminosity function show that A 2163B is dominated by a population of galaxies at redshift  $z \sim 0.2$ , with a spatial distribution characterized by a main central overdensity and a secondary clump at a distance of  $\sim 2'$  from the center. A 2163B turns out, therefore, to be a cluster of galaxies, likely involved in a merging event with A 2163. Galaxies at  $z \sim 0.2$  follow sharp optical–NIR colour-magnitude relations, with slopes that are fully consistent with those expected for a mass-metallicity sequence. The faint end slope of the K-band luminosity function of A 2163B is  $\alpha = -1.2$ , and seems to depend on environment, decreasing from about  $-1$  in the more crowded regions to about  $-1.4$  in the less dense environment. A catalog with all the photometric quantities for the galaxies in the field of A 2163B is provided, including an estimate of the cluster membership obtained by the photometric redshift technique. These information are used in the second paper in order to analyze the structural properties of galaxies at  $z \sim 0.2$ .

**Key words.** Galaxies: clusters: individual: A 2163B – Galaxies: photometry – Galaxies: fundamental parameters

## 1. Introduction

Studies of the galaxy populations in clusters at intermediate redshifts have been proved to be an effective tool to constrain the mechanisms underlying their formation and evolution. A ‘pure photometric’ approach involves the analysis of the galaxy Luminosity Functions (LFs), of the galaxy colours, mainly via the colour-magnitude (CM) diagrams, and of the internal light distribution of galaxies, that is their structural parameters.

The galaxy LF and its dependence on the waveband carry information both on the stellar processes occurring in galaxies and on the cosmological processes which determine the mass function of galaxies. Since Press & Schechter (1974), the shape of the LF has been seen as a basic test of theories of structure formation and evolution. Particularly, the bright end of the LF informs on the properties of massive galaxies, whose formation mechanisms are a lingering debated question. As shown by de Propris et al. (1999) (see also Massarotti et al. 2003 and references therein), the characteristic magnitude of the NIR LF in clusters evolves down to  $z \sim 1$  according to what expected for an old passive stellar population with high formation redshift, implying that massive galaxies are already built up at that redshift. On the other hand, the faint end slope of the LF describes the relative abundance of dwarf galaxies with respect to systems of larger size. Its value and dependence on the environment give valuable information on the physical processes which can affect the population of dwarf galaxies in more dense regions, and are still a matter of debate (e.g. Trentham 1997; de Propris et al. 1998; Andreon 2001; Parolin, Molinari, and Chincarini 2003).

The population of early-type galaxies in clusters follows a tight universal colour-magnitude (CM) relation (Visvanathan & Sandage, 1977; Bower & Lucey, 1992). The slope of this relation shows little evolution over redshift down to  $z \sim 1$ , while its zeropoint changes according to what expected for an old passive stellar population (e.g. Stanford, Eisenhardt, and Dickinson 1998, Kodama et al. 1998, hereafter KAB98). As shown by KAB98 (see also Merluzzi et al. 2003), the evolution of the CM sequence over redshift sets strong constraints on the origin of this relation, resolving the well known age–metallicity degeneracy (Worthey et al., 1996). On the other hand, the fraction of galaxies below the CM sequence appears to be an increasing function of  $z$  (Butcher & Oelmer, 1978). The analysis of the Butcher-Oemler effect is a crucial point to understand the mechanisms by which galaxies are accreted from the field into the dense cluster environment (Kodama & Bower, 2001).

In the framework of a project aimed at investigating the optical–NIR photometric properties of galaxies in the fields of ROSAT PSPC extended sources, we have obtained multi-waveband data (BVRIK) for a field of  $5' \times 5'$  centered at RA = 16h 15m 48s and DEC =  $-06^\circ 02' 10''$ , at

---

*Send offprint requests to:* F. La Barbera

\* Based on observations collected at European Southern Observatory (ESO 65.O-0251, 69.D-0653).  
Tab. 2 is only available in electronic form.

about 6.5' north ( $\sim 1.3$  Mpc at  $z \sim 0.2$  with  $H_0 = 70 \text{ Km s}^{-1} \text{ Mpc}^{-1}$ ,  $\Omega_m = 0.3$  and  $\Omega_\Lambda = 0.7$ )<sup>1</sup> of the Abell cluster A 2163 at redshift  $z = 0.201$  (Arnaud et al., 1994). The coordinates of this field correspond to the center of a secondary extended emission in the X-ray map of A 2163, known as A 2163B (Elbaz, Arnaud, and Böhringer, 1995, hereafter EAB95), with an X-ray temperature  $KT > 6$  keV. The cluster A 2163 (RA = 16h 15m 56s, DEC =  $-06^\circ 08' 55''$ )<sup>2</sup> is a very rich and complex structure of galaxies, which has been extensively studied for its exceptionally hot X-ray temperature,  $KT \sim 12 - 15$  keV (see Markevitch et al. 1996, and references therein), and for its huge radio halo, one of the most powerful known so far (Feretti et al., 2001, hereafter FFG01). It has also been the subject of various studies on the Sunyaev–Zeldovich effect (see Colafrancesco, Marchegiani, and Palladino 2003, and references therein). On the contrary, the properties of the galaxy population of this cluster have actually remained unexplored (but see Squires, Neumann, and Kaiser 1997). Our data show the presence of a significant excess of galaxies at redshift  $\sim 0.2$  in the field of A 2163B, with a NIR spatial distribution typical for a cluster of galaxies, with a main central overdensity and a secondary structure at  $\sim 0.4$  Mpc in the north-east direction. A 2163B turns out, therefore, to be a cluster of galaxies likely involved in a merging event with A 2163.

The present work is the first of two papers aimed at studying the photometric and structural properties of the galaxy population of A 2163B. In the present study (paper I), we discuss the integrated photometric properties of galaxies at  $z \sim 0.2$ , providing a catalog that includes magnitudes, colours and structural parameters for the galaxies in the field of A 2163B. In paper II (La Barbera et al., 2003a), we analyze the structural properties of galaxies at  $z \sim 0.2$ , by studying the internal colour gradients of galaxies and the correlations between structural parameters.

The layout of the paper is as follows. Observations and data reduction are described in Secs. 2 and 3. The luminosity density map, the colour-magnitude relations and the K-band luminosity function of A 2163B are studied in Sec. 4. In the same section, a new method based on the optical–NIR CM relations is presented to estimate both the cluster redshift and the galactic reddening towards the field of A 2163B. Cluster members are then selected by the photometric redshift technique, as described in Sec. 5, and the photometric catalog of A 2163B is presented in Sec. 6. Conclusions are drawn in Sec. 7.

## 2. Observations

The data relevant for the present study were collected at the ESO New Technology Telescope and include BVRIK photometry centered on the field of galaxies A 2163B. The data were obtained on August and September 2000 (hereafter run I), under partly non photometric conditions, and on April 2002 (hereafter run II), under photometric conditions.

<sup>1</sup> We will adopt this cosmology throughout the paper. With these parameters the age of the universe is  $\sim 13.5$  Gyr, and the redshift 0.2 corresponds to a lookback time of  $\sim 2.5$  Gyr.

<sup>2</sup> The coordinates refer to J2000 and define the peak of the X-ray emission (Elbaz, Arnaud, and Böhringer, 1995).

**Table 1.** Observations. The notes refer to the sky conditions: NP and P denote non-photometric and photometric conditions, respectively.

| Run       | Date           | Note | Waveband | $N_{\text{exp}}$ | $T_{\text{exp}}$<br>(s) | FWHM<br>( $''$ ) |
|-----------|----------------|------|----------|------------------|-------------------------|------------------|
| <i>I</i>  | 25/08/2000     | NP   | V        | 3                | 900                     | 1.3              |
| <i>I</i>  | 24/08/2000     | NP   | R        | 2                | 450                     | 1.0              |
| <i>I</i>  | 26/08/2000     | NP   | I        | 2                | 450                     | 1.0              |
| <i>I</i>  | 08, 10/09/2000 | P    | K        | 70               | 60                      | 0.6 – 1.0        |
| <i>I</i>  | 09/09/2000     | NP   | K        | 50               | 60                      | 1.0              |
| <i>II</i> | 09/04/2002     | P    | B        | 2                | 300                     | 1.5              |
| <i>II</i> | 09/04/2002     | P    | V        | 1                | 300                     | 1.2              |
| <i>II</i> | 09/04/2002     | P    | R        | 1                | 300                     | 0.9              |
| <i>II</i> | 09/04/2002     | P    | I        | 1                | 300                     | 1.0              |

During three nights of run I, we obtained K-band imaging with the SOFI instrument (pixel scale  $0.288''/\text{pxl}$ ) for a field of  $5' \times 5'$ . The sky conditions were photometric for two nights and non photometric for the third night. A total of 120 exposures were collected, with a DIT value of 6 s, NDIT = 10, and a dithering box of  $18''$ . Due to the non photometric conditions, only 85 exposures were retained, resulting in a total integration time of 5100 s. Standard stars from Persson et al. (1998) were observed during each night, each at five different positions on the chip. In order to perform the illumination correction (see Sec. 3.2), we also observed a standard star at different positions on a  $5 \times 5$  grid across the frame. In the same period, we also obtained V-, R-, and I-band photometry with the EMMI instrument for a region of  $8.6' \times 8.6'$  (pixel scale  $0.267''/\text{pxl}$ ), under non photometric conditions. On April 2002, the field A 2163B was re-observed in B, V, R and I bands with EMMI under photometric conditions. The relevant information on the observations are summarized in Tab. 1. The total exposure times amount to 600, 2700, 1200 and 1200 s for the B, V, R and I bands, respectively.

### 3. Data reduction

The data were reduced by using FORTRAN routines developed by the authors and IRAF packages<sup>3</sup>. Details are given in Secs. 3.1 and 3.2 for the optical and the NIR images, respectively.

<sup>3</sup> IRAF is distributed by the National Optical Astronomy Observatories, which are operated by the Association of Universities for Research in Astronomy, Inc., under cooperative agreement with the National Science Foundation.

### 3.1. *BVRI data*

Both the images of the first and of the second run were reduced by following the same procedure. After bias subtraction, the images were divided by a flat-field frame obtained by combining twilight sky exposures. Since this procedure did not fully remove low frequency variations of the background across the images (at level of  $\sim 5\%$ ), we obtained a super-flat correction for each band by median combining the corresponding scientific exposures. A polynomial fit was applied to each super-flat frame and the fitted surfaces were used to correct the scientific exposures. This procedure reduced background variations in the final images at the level of  $\sim 0.5\%$ . After flat-field, the cosmic rays in each exposure were detected by using the IRAF task COSMICRAYS, and a mask frame was constructed including hot pixels and the bad columns. The images of each run were then combined by using the IRAF task IMCOMBINE. Since only run II was photometric, the images of run I were suitably scaled and combined with those of run II. The scaling factors were computed from the mean difference of the magnitudes of bright unsaturated stars in the observed field. The seeing FWHM is  $1.5''$ ,  $1.2''$ ,  $1.0''$  and  $1.0''$  for the B, V, R, and I bands, respectively. The images were calibrated into the Johnson-Kron-Cousins photometric system by using standard stars from Landolt (1992). Since comparison fields for different airmasses were not available, we adopted the extinction coefficients typical for the site of La Silla:  $A_B = 0.21$ ,  $A_V = 0.13$ ,  $A_R = 0.09$ ,  $A_I = 0.05$  mag/airmass. Instrumental magnitudes for the Landolt stars were computed within an aperture of diameter  $10''$  by means of SExtractor (Bertin & Arnout, 1996). For each band, in order to obtain the zero-point and the colour term of the photometric calibration, we performed a robust least square fit. Colour terms were found to be small and were neglected, while the zeropoints turned out to be  $ZP_B = 24.31 \pm 0.01$ ,  $ZP_V = 24.92 \pm 0.01$ ,  $ZP_R = 25.06 \pm 0.01$ ,  $ZP_I = 24.41 \pm 0.01$  mag (scaled to 1 s exposure time).

### 3.2. *K-band data*

For each dithering sequence, the exposures were dark subtracted and corrected for flat-field, using a super flat frame obtained by median combining all the images taken during the night. After this procedure, the magnitudes of the standard stars showed a rms variation across the chip of  $\sim 0.04$  mag. To achieve a better accuracy, we obtained an illumination correction frame by measuring the magnitude of a standard star at different positions in a  $5 \times 5$  grid on the frame. All the images were divided by the illumination correction frame, which allowed the low frequency component of the flat-field to be corrected at better than 1%. Since sky subtraction is a very troublesome step for the reduction of NIR data, particularly in high density regions mostly populated by bright early-type galaxies with extended halos, this point was carefully dealt with by a two step procedure. First, each exposure was sky subtracted by computing the sky frame from the median of the six closest frames along the sequence. The images were then registered with integer shifts and combined, with a sigma clipping algorithm for cosmic ray rejection. This

procedure, however, overestimate the sky level in the extended halos of galaxies, and therefore, it is not suitable to derive the surface photometry (paper II). For this reason, we reiterated the sky subtraction, proceeding as follows. The first step combined images were used to obtain mask frames for the sources in the field, by running SExtractor with the checkimage OBJECTS option. For each sequence, the mask was expanded in order to 'cover' the galaxy halos and was de-registered to each dithered exposure, by including also hot and bad pixels. The sky frames were estimated by an average of the six closest frame for the exposures of each sequence, rejecting masked pixels. The images were then sky subtracted and combined with IMCOMBINE<sup>4</sup> (using the SIGCLIP option), resulting in a final image with a seeing FWHM of  $\sim 0.9''$ . The photometric calibration was performed into the Ks standard filter (Persson et al., 1998), deriving the instrumental magnitudes of the standard stars within an aperture of diameter  $8''$ . The airmass correction was performed by using an extinction coefficient  $A_K = 0.06$  mag/airmass, which was derived by comparing the magnitudes of bright objects in the field for different airmasses. The K-band zeropoint turned out to be  $ZP_K = 22.422 \pm 0.015$  mag (scaled to 1 s exposure time).

### 3.3. Aperture photometry

Photometry was derived by using the software SExtractor. For the optical images, SExtractor was run in the so-called double correlated mode, using the R-band image for the detection of the sources, and the other images only to measure their fluxes. Particular care was taken so that closed objects were deblended in the same way both in the optical and in the NIR images. The BVRI and the K-band catalogs were cleaned by spurious detections and cross-correlated. For each object, we computed colour indices by using magnitudes within a fixed aperture of diameter  $3.5''$ , corresponding to  $\sim 12$  kpc at redshift  $z = 0.2$ . Since the images have different seeing, the aperture magnitudes were corrected to the same FWHM of  $1.2''$ , following the procedure detailed in La Barbera et al. (2003b). The aperture corrections amount to  $-0.04$ ,  $0.$ ,  $0.02$ ,  $0.02$ , and  $0.04$  mag for the B, V, R, I and K bands, respectively. Total magnitudes were obtained with the SExtractor mag-auto parameter, which provides magnitudes in an adaptive aperture of diameter  $\alpha \cdot r_K$ , where  $r_K$  is the Kron (1998) radius, and  $\alpha = 2.5$ , for which the Kron magnitude encloses 94% of the object source. Total magnitudes<sup>5</sup> were then obtained by subtracting 0.06 mag from the Kron magnitudes. Galaxy/star separation was performed on the basis of the stellar index SG of SExtractor, defining as stars the objects with  $SG \geq 0.97$ . For the K band, the completeness magnitude is  $K_T = 19$ , and was estimated by following the method of Garilli, Maccagni, and Andreon (1999). Down to this limit, the BVRIK catalog includes  $N = 317$  galaxies. The completeness of the BVRIK catalog with respect to the K-band catalog is  $\sim 98\%$  at  $K_T = 17.5$ , falling to  $\sim 90\%$  at  $K_T = 19$ . For the optical catalogs, we also computed the fraction of sources for which SExtractor provides reliable magnitude estimates<sup>6</sup> as a function of the K-band magnitude. For the B band,

<sup>4</sup> The images taken under non-photometric conditions were suitably scaled to the others.

<sup>5</sup> In the following, total magnitudes will be indicated by a pedex T.

<sup>6</sup> We adopted an upper limit of 100% for the uncertainty on the flux.

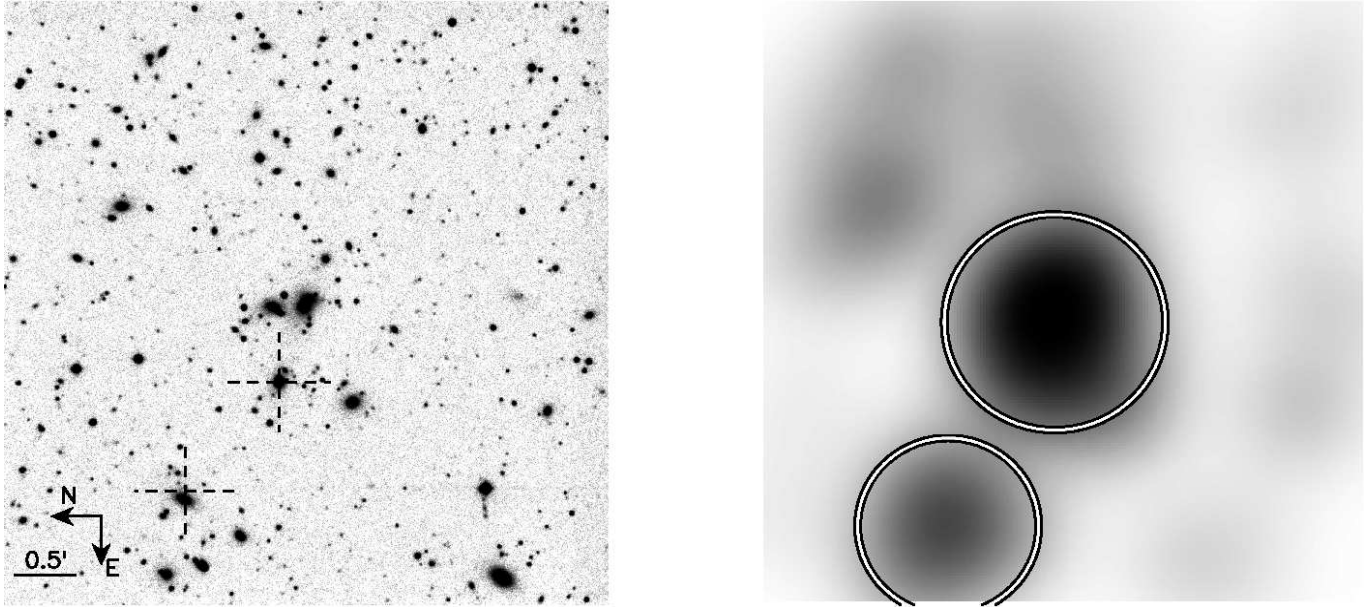


**Fig. 1.** K-band image (left panel) and luminosity-weighted map (right panel) for the field of galaxies A 2163B. The image is centered at RA = 16h 15m 48s and DEC =  $-06^{\circ} 02' 10''$ , and was smoothed for the plot by a gaussian convolution. The scale and the orientation of the image are shown in the lower left corner of the left panel. In the same panel, the crosses indicates the positions of the radio sources in the field. In the right plot, the circles enclose the regions that were used to calculate the luminosity function in the higher density environment (see Sec. 4.2).

this fraction  $f_S$  amounts to  $\sim 90\%$  at  $K_T = 17.5$ , dropping to  $\sim 0.5$  at  $K_T = 19$ . For the V, R and I bands, we have  $f_S(K_T = 17.5) = 0.95, 0.98, 0.98$  and  $f_S(K_T = 19) = 0.76, 0.84, 0.88$ , respectively.

#### 4. The cluster A 2163B

Fig. 1 plots the K-band image of A 2163B and the luminosity-weighted density map for the  $N = 105$  galaxies brighter than  $K_T = 17$ . The figure clearly shows the presence of a cluster of galaxies, with a main over-density in the center and a secondary structure at a distance of  $\sim 2'$  ( $\sim 0.4$  Mpc) from the main peak. We note that, on the basis of field galaxy counts (Sec. 4.2), only  $\sim 15$  galaxies out of 105 are expected to be field contaminants in the area of the K-band image, confirming that the features in Fig. 1 (right panel) are highly significant. It is very interesting to note that both the X-ray image of A 2163B and the 20 cm radio map show a spatial structure very similar to the luminosity density image (see Fig. 7 of FFG01). In Fig 1, we also show the positions of the two radio sources found by FFG01. One of this turns out to coincide with an early-type<sup>7</sup> galaxy (possible merging) in the main clump, while the second is very close to a bright early-type in the second overdensity region. A reliable estimate of the redshift  $z_c$  of the galaxy population of A 2163B can be obtained by using purely photometric techniques. In the following, we will

<sup>7</sup> Sersic index greater than 2.

estimate  $z_c$  by studying (1) the optical–NIR colour magnitude (hereafter CM) relations (Sec. 4.1) and (2) the K-band luminosity function (Sec. 4.2). Since the field of A 2163B is characterized by a high galactic reddening, the derivation of  $z_c$  and the study of the photometric properties of the galaxy population require an accurate estimate of  $E(B - V)$ . The main sources for the reddening of the Milk Way are based on HI measurements from Burstein & Heiles (1984, hereafter BH84) and on COBE/DIRBE and IRAS/ISSA FIR data from Schlegel, Finkbeiner, and Davis (1998, hereafter SFD98). Generally, the estimates of  $E(B - V)$  from SFD98 are systematically higher with respect to those of BH84. For A 2163B, BH84 and SFD98 predict very different extinction values,  $E(B - V) = 0.18$  and  $E(B - V) = 0.415$ , respectively. However, as shown in the next section, an accurate estimate of the galactic reddening as well as of the cluster redshift can be determined from the optical–NIR colour magnitude relations, taking advantage of the large wavelength baseline provided by the BVRIK photometry. Therefore, the above difference of reddening values does not affect the present analysis.

#### 4.1. Colour magnitude relations

Fig. 2 shows the optical–NIR CM diagrams, not corrected for galactic extinction, for all the galaxies brighter than  $K_T = 18.6$  in the field of A 2163B. Each diagram shows a sharp sequence of red galaxies, following the CM relation:

$$N - K = \Gamma_{K_r} + \Delta \cdot (K_T - K_r) \quad (1)$$

where  $N$  is the optical waveband,  $K_r$  is a reference K-band magnitude,  $\Delta$  is the slope and  $\Gamma_{K_r}$  is the zeropoint of the relation, that is the  $N - K$  colour at  $K_T = K_r$ . The values of  $\Gamma_{K_r}$  and  $\Delta$ , that are reported in Fig. 2, were estimated by applying a least square fit, minimizing the rms of the residuals in colour,  $\sigma_{N-K}$ , to the relation. In order to reduce the effect of outliers and field contaminants, the value of  $\sigma_{N-K}$  was computed by using the bi-weight statistics (Beers, Flynn, and Gebhardt, 1990). Moreover, for comparison with previous works (Kodama et al., 1998, hereafter KAB98), the fits were performed by considering only the galaxies within the three brightest magnitudes of the red sequence, corresponding to  $K_T \lesssim 16.5$ . We note that, down to this limit, the BVRIK photometry is complete (see Sec. 3.3), and that, on the basis of field galaxy counts (see Sec. 4.2), only  $\sim 10\%$  of the galaxies are expected to be field contaminants. Despite the large uncertainties, the values of  $\Delta$  show that the slope of the CM relation decreases systematically from about  $-0.1$  for the B–K sequence to about  $-0.04$  for the I–K relation. The slopes of the V–K, R–K and I–K sequences can be straightly compared with those predicted from a pure mass-metallicity model by KAB98 at the redshift of A 2163B ( $z \sim 0.2$ , see below):  $\Delta_{V-K} = -0.075$ ,  $\Delta_{R-K} = -0.062$ , and  $\Delta_{I-K} = -0.05$  (see their Fig. 4). Our results confirm those values.

For what concerns the zeropoints of the CM relations, they can be used to estimate simultaneously the cluster redshift and the reddening of the Galaxy in the direction of A 2163B. To this aim, we fitted the values of  $\Gamma_{K_r}$  with those expected for an old, passively evolving, stellar population (hereafter SP), as a function of the redshift  $z$  and of the reddening  $E(B - V)$ . We also

accounted for the metallicity change of the galaxy SPs along the CM sequence, proceeding as follows. As shown by Merluzzi et al. (2003), the CM relation is reproduced by the metallicity–luminosity relation:

$$\log(Z/Z_{\odot}) = (-0.097 \pm 0.005) \cdot M_V + (-2.09 \pm 0.09), \quad (2)$$

where  $M_V$  is the absolute V-band magnitude. Using the slope of the CM relation for nearby early-types from Bower & Lucey (1992), the above relation allows the absolute K-band magnitude to be estimated for a given metallicity  $Z$ . For  $Z = Z_{\odot}$ , we obtain  $K(Z_{\odot}) = K_{\odot} = -24.74 \pm 0.15$ . In order to predict the value of  $K(Z_{\odot})$  as a function of redshift ( $K_{\odot}(z)$ ), we have to take into account the luminosity distance term, and the K+E corrections. To this aim, we used galaxy templates from the GISSSEL00 code (Bruzual & Charlot, 1993), with a Scalo IMF, an exponential star formation rate  $\exp(-t/\tau)$  and solar metallicity. These models were also used to predict (1) the optical–NIR galaxy colours as a function of the redshift  $z$ , and (2) the absorption coefficients  $A_N$  and  $A_K$  as a function of  $z$  and  $E(B - V)$ , using the extinction law from SFD98. The values of  $z_c$  and  $E(B - V)$  were derived by minimizing the following expression:

$$\chi^2[z_c, z_f, E(B - V)] = \sum_N [\Gamma_{K_{\odot}(z)} - (N - K)_t + (A_N - A_K)]^2 \quad (3)$$

where  $(N - K)_t$  are the template colours, and  $z_f$  is the formation redshift, which was allowed to vary in the range  $[1.2, 10]$ . The uncertainties on  $z_c$  and  $E(B - V)$  were obtained by shifting the values of  $\Gamma_{K_{\odot}(z)}$  according to the relative uncertainties and re-iterating the  $\chi^2$  minimization. The procedure was repeated by using galaxy templates with two  $\tau$  values:  $\tau = 0.01$  Gyr, which describes a SSP, and  $\tau = 1$  Gyr corresponding to a star formation rate that lasts longer in time. The best-fit values turned out not to vary significantly between the two cases:  $z_c = 0.215 \pm 0.015$  and  $E(B - V) = 0.41 \pm 0.02$ . It is remarkable that the above procedure gives an  $E(B - V)$  estimate which is in very good agreement with that of SFD98 ( $E(B - V) = 0.415$ ), proving that SFD98 provide a reliable value of the galactic reddening for the field of A 2163B. For this reason, we assumed  $E(B - V) = 0.415$  in the following, and applied the corresponding absorption corrections to our photometry<sup>8</sup>. Repeating the  $\chi^2$  minimization with  $E(B - V) = 0.415$  gives  $z_c = 0.21 \pm 0.01$ , which is the final redshift estimate of the A 2163B galaxy population.

## 4.2. Luminosity function

The evolution of the characteristic magnitude  $K^*$  of the K-band luminosity function (LF) of cluster galaxies at  $z \lesssim 1$  is consistent with the behaviour of an old passive stellar population with formation redshift  $z_f \in [2, 3]$  and solar metallicity. This result was obtained by de Propris et al. (1999, hereafter dPS99) fitting a Schechter function (hereafter SF) with fixed slope  $\alpha = -0.9$  to the K-band counts of cluster galaxies with  $K_T - K^* < 3$ , and turns out to be independent of cluster richness or X-ray luminosity. We used these results in order to obtain a fur-

<sup>8</sup> For  $E(B - V) = 0.415$ , at  $z \sim 0.2$ , and practically for any galaxy spectral model, we have  $A_B = 1.630$ ,  $A_V = 1.281$ ,  $A_R = 1.049$ ,  $A_I = 0.788$  and  $A_K = 0.152$ .

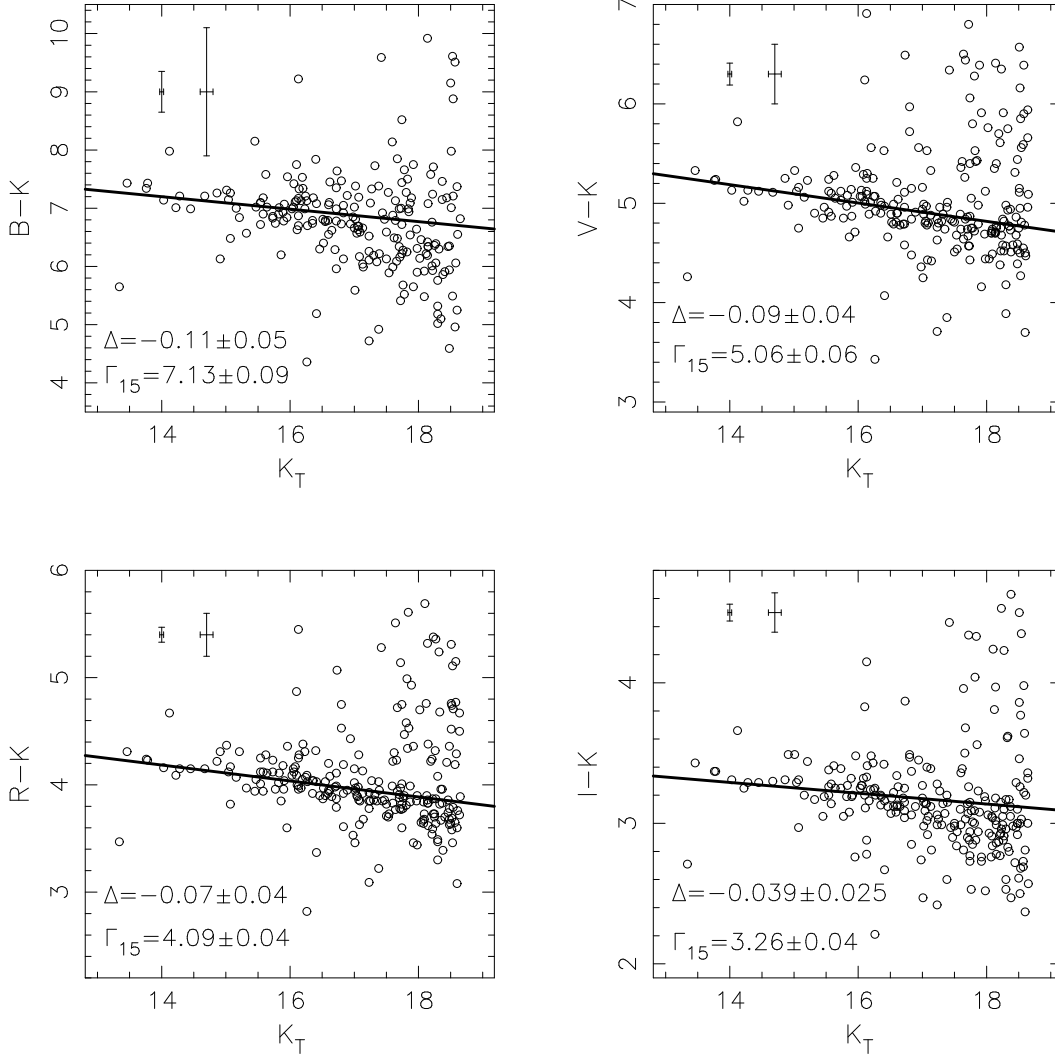


**Fig. 2.** Optical–NIR CM diagrams for galaxies in the field of A 2163B. For each panel, the slope and zero-point of the CM relations are shown in the lower left corner, while the error bars from the left to the right denote the averaged uncertainties on colours and magnitudes at  $K_T = 15$  and  $K_T = 18$ , respectively.

ther estimate of the redshift of A 2163B. The K-band LF was obtained by correcting our number counts with field galaxy counts from the Calar Alto Deep Imaging Survey (CADIS, see Huang, Thompson, and Kümmel 2001), which is the largest medium deep K-band survey to date, with a total area of  $0.2 \text{ deg}^2$  and a completeness magnitude of 19.75 mag. Since our K-band photometry is complete down to  $K_T = 19$ , the CADIS data are the most suitable dataset for the estimate of field galaxy counts. The LF of A 2163B is shown in Fig. 3. The error bars take into account Poissonian uncertainties on both field and cluster counts, while the different curves show the SF fits of the LF. In order to account for the finite size of the magnitude bins, the fits were performed by the convolution of a SF with the bin size. Following dPS99 and de Propris & Pritchett (1998, hereafter dPE98), we fitted the galaxy counts down to  $K_T = 18$ . ( $\sim K^* + 3$ , see below) by a SF with  $\alpha = -0.9$ , excluding the three brightest cluster galaxies. The fit provided a good

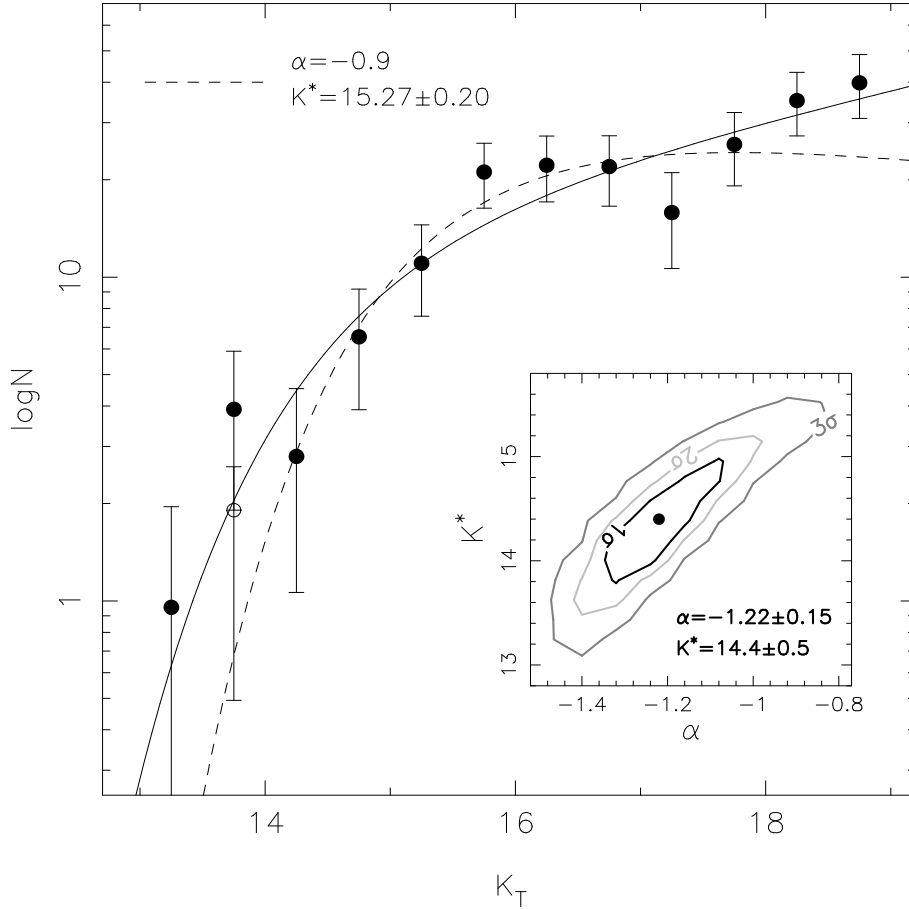


**Fig. 3.** K-band luminosity function of A 2163B. The two curves indicate the best-fit Schechter functions obtained by fitting both  $\alpha$  and  $K^*$  (solid line) and by fitting only  $K^*$  with  $\alpha$  fixed to  $-0.9$  (dashed line). In the last case, the three brightest cluster galaxies were excluded from the fit: the first bin was not considered while the galaxy counts for the second bin are marked by the empty circle. Contours in the smaller panel denote  $1\sigma$ ,  $2\sigma$  and  $3\sigma$  probability levels, respectively.

description of the counts of bright galaxies<sup>9</sup>, giving the following estimate of the characteristic magnitude:  $K_{0.9}^* = 15.3 \pm 0.20$ . In order to estimate  $z_c$ , we minimized the function:

$$\chi^2 = [K_{0.9}^*(z) - K_{0.9}^*]^2, \quad (4)$$

where  $K_{0.9}^*(z)$  is value of  $K^*$  expected at redshift  $z$ , and was obtained by adding to the value of the characteristic magnitude of the Coma cluster ( $10.9 \pm 0.2$ , see dPE98) the luminosity distance term and the K+E corrections, derived from GISSSEL00 spectral models with a Scalo IMF and an exponential SFR. It turned out that, by using models with different metallicities ( $Z/Z_\odot = 0.5, 1., 2.$ ) and formation redshifts ( $z_f \geq 1.5$ ), the estimate of  $z_c$  does not vary significantly:  $z_c = 0.20 \pm 0.02$ . This result is in very good agreement with that obtained from the CM relations in Sec. 4.1. We found that the estimate of  $z_c$  is very robust with respect to the field subtraction

<sup>9</sup> The only two bins for which galaxy counts deviate by more than  $1\sigma$  from the model are at  $K_T > 17$ . We note that limiting the fit range to  $K_T < 17$  does not affect our results, giving  $K_{0.9}^* = 15.34 \pm 0.2$ .

procedure and to the value adopted for the galactic reddening, due to the low sensitivity of the K-band photometry to dust absorption. For example, by using  $E(B - V) = 0$ , we obtain  $z_c = 0.225$ , and neglecting field counts gives  $z_c = 0.21$ .

In order to study the faint end of the LF, we performed a SF fit for  $K_T < 19$  by treating both  $\alpha$  and  $K^*$  as free parameters. As shown in Fig. 3, the SF, whose best-fit parameters are  $\alpha = -1.22 \pm 0.15$  and  $K^* = 14.45 \pm 0.50$ , provides a good description of the LF of A 2163B. Only for the two bins at  $K_T = 15.75$  and  $K_T = 17.25$  the cluster counts show some deviation from the SF fit. Although this could be an indication for a bimodal behaviour of the LF, as found by previous studies (see Mercurio et al. 2003, and references therein), the deviations are only at the levels of  $1.6\sigma$  and  $1.7\sigma$ , respectively, and are therefore not statistically significant. The value of  $\alpha$  is in very good agreement with the value of  $-1.18$  found by Andreon (2001) for a rich cluster of galaxies at  $z = 0.3$  in an area of  $\sim 1.3 \text{ Mpc}^2$ , which is similar to that analyzed in the present study ( $\sim 1 \text{ Mpc}^2$ ), and is also consistent with values of the faint end slope of the NIR LF for the Coma cluster,  $\alpha = -1.0$  (dPE98) and  $\alpha = -1.3$  (Andreon & Pellò, 2000), and for field galaxies,  $\alpha = -1.09$  (Kochanek et al., 2001). We also attempted to analyze the dependence of the LF of A 2163B on environment, by performing the SF fits separately for the galaxies inside an higher density region, defined by the circles in Fig. 1, and for the galaxies outside that region. Interestingly, the values of  $\alpha$  vary from  $-0.96 \pm 0.18$  (higher density) to  $-1.4 \pm 0.2$  (lower density), suggesting a steepening of the faint end slope at lower densities, in agreement with the findings of previous studies (e.g. Andreon 2001).

## 5. Photometric redshifts

In order to select cluster members, we used the photometric redshift technique, proceeding as in Busarello et al. (2002) and La Barbera et al. (2003b). Photometric redshifts were estimated according to the Spectral Energy Distribution fitting method (see Massarotti, Iovino, and Buzzoni 2001a; Massarotti et al. 2001b, and references therein). In order to achieve a reasonable accuracy, we considered galaxies with signal-to-noise ratio  $S/N > 5$  in at least three bands, limiting the sample to the  $N = 131$  galaxies brighter than  $K_T = 17.75$  (not corrected for extinction of the Galaxy). Since the percentage of galaxies at redshift  $z > 1$  with  $K < 17.5$  is expected to be negligible<sup>10</sup> ( $< 2\%$ ), we looked for redshifts in the range  $z \in [0.0, 1.0]$  with a step of 0.01, imposing that at a given redshift galaxy templates were younger than the age of the universe in the adopted cosmology. We used the GISSEL00 code in order to produce galaxy templates with a Scalo IMF and an exponential SFR  $e^{-t/\tau}$ . The colours of E/S0, Sa/Sb, and Sc/Sd spectra were modeled by choosing  $\tau = 1, 4$  and  $15 \text{ Gyr}$ , respectively, while early-type galaxies with different metallicities were described by using E/S0 models with  $Z/Z_\odot = 0.2, 0.4, 1$  and  $2.5$ . The differential dust extinction of the Milk Way was included in the computation of model colours by adopting

<sup>10</sup> This estimate was obtained by using a Pure Luminosity Evolution model (see e.g. Pozzetti, Bruzual, and Zamorani 1996).

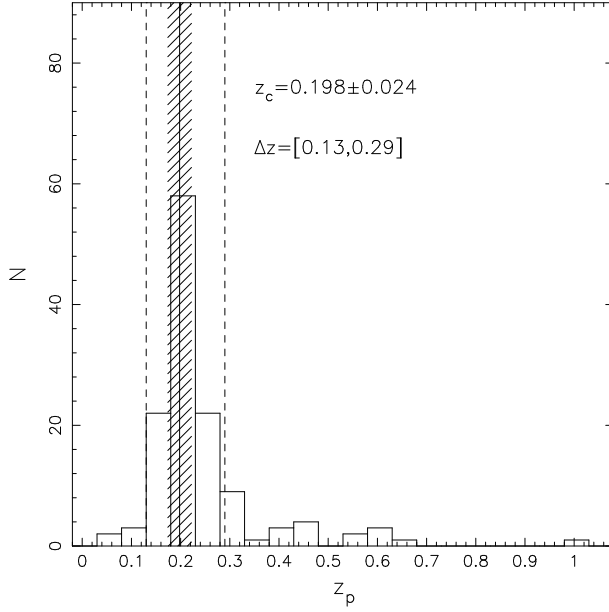


**Fig. 4.** Distribution of photometric redshifts. The solid line and the dashed region indicate the estimate of the cluster redshift,  $z_c$ , and the relative uncertainty ( $1\sigma$  standard interval). Dashed lines enclose the range of  $z_p$ ,  $\Delta z$ , used to select cluster members.

the extinction curve of SFD98 and a colour excess of  $E(B - V) = 0.415$  (see Sec. 4.1). The uncertainty on the photometric redshift  $\delta z$  was estimated by performing numerical simulations, taking into account the measurement errors on galaxy colours. The mean value of  $\delta z$  is  $\sim 0.08$ , varying from  $\sim 0.05$  at  $K_T = 15$  to  $\sim 0.1$  at  $K_T = 17$ .

As shown in Fig. 4, the distribution of photometric redshifts is dominated by the peak around  $z \sim 0.2$ , indicating that most galaxies with  $K_T < 17.5$  are actually cluster members. Applying the bi-weight statistics, we obtained the following estimate of the cluster redshift:  $z_c = 0.198 \pm 0.024$ , in agreement with the values obtained in Sec. 4.1 and 4.2. Galaxies with photometric redshift in a range of  $2\overline{\delta z}$  around  $z_c$  ( $z_c = 0.21$ , see Sec. 4.1) were defined as cluster members, resulting in a final list of  $N = 102$  objects. This value is in good agreement with that predicted on the basis of field galaxy counts,  $N = 112$  (see Sec. 4.2).

## 6. Description of the catalog

The catalog includes the BVRIK photometric quantities for the  $N = 131$  galaxies for which we obtained photometric redshift estimates. A portion of the catalog<sup>11</sup> is shown in Tab. 6. The catalog is organized as follows.

Two rows correspond to each galaxy. The first one provides the measured quantities, while the second one gives the relative uncertainties (one sigma standard intervals). All the photometric quantities have been corrected for galactic extinction by using the photometric redshift estimates and adopting  $E(B - V) = 0.415$ . The typical uncertainties on the structural parameters are dis-

<sup>11</sup> The full catalog will be available in electronic form at the CDS via anonymous ftp to cdsarc.u-strasbg.fr.

cussed in paper II.

Column 1: running number of the catalog.

Column 2: photometric redshift.

Column 3, 4: right ascension and declination referred to J2000. The astrometric solution was computed by using a list of stars from the USNO catalog. The rms of the residuals to the astrometric solution is  $0.2''$ .

Columns 5–9: B-, V-, R-, I- and K-band total magnitudes.

Columns 10–13: optical–NIR galaxy colours in the aperture of  $3.5''$  corrected for seeing effects.

Columns 14–16: mean surface brightness  $\langle\mu\rangle_e$  within the effective radius  $r_e$ , logarithm of  $r_e$  (in arcsec) and Sersic index  $n$  for the R-band.

Columns 17–19: the same of columns 14–16 for the I-band.

Columns 20–22: the same of columns 14–16 for the K-band.

Columns 23, 24: axis ratio and position angle in degree obtained from the K-band surface photometry.

## 7. Conclusions

We have studied the integrated photometric properties of the galaxy population in a field centered around the X-ray extended source A 2163B, near the cluster A 2163 ( $z = 0.201$ ). The BVRIK data-set has been presented, including galaxy celestial coordinates, magnitudes, colours, photometric redshifts and the structural parameters, which will be discussed in paper II.

The K-band image of A 2163B shows the presence of a cluster of galaxies, with a main central clump of diameter  $\sim 0.4$  Mpc, and a secondary structure at a distance of  $\sim 0.4$  Mpc from the center. The colour-magnitude diagrams show the presence of a sharp sequence of red galaxies, with a slope that flattens at longer wavelengths: galaxy colours become bluer by  $\sim 0.1$  mag per magnitude in the B – K vs.  $K_T$  diagrams, and by  $\sim 0.04$  mag into the I – K vs.  $K_T$  plane. The slopes of the sequences are consistent with those predicted by Kodama et al. (1998), for a model in which the CM relation mainly originates from a mass–metallicity sequence. By introducing a suitable procedure which allows the cluster redshift,  $z_c$ , and the Milk Way reddening to be simultaneously estimated, we obtain a redshift of  $\sim 0.2$  for the galaxy population of A 2163B, which turns out, therefore, to be likely a cluster of galaxies involved in a merging event with A 2163. The value of  $z_c$  is also confirmed by the analysis of the K-band luminosity function and by the photometric redshift technique, which is employed to select cluster members.

The luminosity segregation of A 2163B is more deeply investigated by means of the K-band luminosity function. The global LF is well described by a single Schechter function with a faint end slope of  $\alpha = -1.2$ , which is consistent with values found by other studies of the NIR LF both in cluster and in the field (e.g. Andreon 2001; Andreon & Pellò 2000; Kochanek et al. 2001). The faint end slope, however, seems to depend on environment, varying from about  $-1$  in the

| #   | $z_p$ | RA          | DEC        | $B_T$ | $V_T$ | $R_T$ | $I_T$ | $K_T$ | $B - K$ | $V - K$ | $R - K$ | $I - K$ | $\langle \mu \rangle_e^R$ | $\log r_e^R$ | $n^R$ | $\langle \mu \rangle_e^I$ | $\log r_e^I$ | $n^I$ | $\langle \mu \rangle_e^K$ | $\log r_e^K$ | $n^K$ | $b/a$ | $PA$   |
|-----|-------|-------------|------------|-------|-------|-------|-------|-------|---------|---------|---------|---------|---------------------------|--------------|-------|---------------------------|--------------|-------|---------------------------|--------------|-------|-------|--------|
| (1) | (2)   | (3)         | (4)        | (5)   | (6)   | (7)   | (8)   | (9)   | (10)    | (11)    | (12)    | (13)    | (14)                      | (15)         | (16)  | (17)                      | (18)         | (19)  | (20)                      | (21)         | (22)  | (23)  | (24)   |
| 1   | 0.12  | 16:15:57.88 | -6:03:59.3 | 17.05 | 16.07 | 15.57 | 15.08 | 13.18 | 4.01    | 3.03    | 2.51    | 2.05    | ...                       | ...          | ...   | ...                       | ...          | ...   | ...                       | ...          | ...   | ...   | ...    |
|     | 0.05  |             |            | 0.06  | 0.03  | 0.02  | 0.02  | 0.01  | 0.18    | 0.15    | 0.15    | 0.15    |                           |              |       |                           |              |       |                           |              |       |       |        |
| 2   | 0.62  | 16:15:58.16 | -6:03:44.2 | 25.69 | 21.17 | 20.04 | 19.06 | 15.97 | 7.58    | 5.68    | 4.49    | 3.50    | ...                       | ...          | ...   | ...                       | ...          | ...   | ...                       | ...          | ...   | ...   | ...    |
|     | 0.13  |             |            | 20.22 | 0.25  | 0.13  | 0.10  | 0.03  | 2.03    | 0.41    | 0.26    | 0.23    |                           |              |       |                           |              |       |                           |              |       |       |        |
| 3   | 0.19  | 16:15:57.79 | -6:01:12.7 | 19.49 | 17.93 | 17.24 | 16.67 | 14.13 | 5.58    | 3.91    | 3.20    | 2.65    | 21.14                     | 0.439        | 5.27  | 20.57                     | 0.449        | 5.26  | 17.21                     | 0.278        | 5.76  | 0.880 | -92.05 |
|     | 0.01  |             |            | 0.18  | 0.06  | 0.04  | 0.03  | 0.02  | 0.29    | 0.16    | 0.15    | 0.15    |                           |              |       |                           |              |       |                           |              |       |       |        |
| 4   | 0.17  | 16:15:57.31 | -6:01:27.0 | 20.99 | 19.28 | 18.68 | 17.99 | 15.62 | 5.10    | 3.63    | 3.00    | 2.39    | 19.94                     | -0.220       | 3.18  | 19.40                     | -0.225       | 2.86  | 16.89                     | -0.185       | 3.02  | 0.637 | -84.44 |
|     | 0.05  |             |            | 0.38  | 0.10  | 0.07  | 0.06  | 0.03  | 0.42    | 0.22    | 0.19    | 0.19    |                           |              |       |                           |              |       |                           |              |       |       |        |
| 5   | 0.46  | 16:15:57.41 | -6:03:24.5 | 23.67 | 20.94 | 19.83 | 19.09 | 15.95 | 6.12    | 5.03    | 3.92    | 3.19    | ...                       | ...          | ...   | ...                       | ...          | ...   | ...                       | ...          | ...   | ...   | ...    |
|     | 0.06  |             |            | 2.40  | 0.22  | 0.11  | 0.10  | 0.03  | 0.73    | 0.31    | 0.22    | 0.21    |                           |              |       |                           |              |       |                           |              |       |       |        |
| 6   | 0.21  | 16:15:57.69 | -6:01:09.7 | 21.50 | 19.85 | 19.25 | 18.67 | 16.43 | 5.15    | 3.58    | 2.96    | 2.42    | 20.90                     | -0.222       | 4.76  | 20.39                     | -0.201       | 4.54  | ...                       | ...          | ...   | ...   | ...    |
|     | 0.06  |             |            | 0.53  | 0.13  | 0.09  | 0.08  | 0.04  | 0.60    | 0.26    | 0.23    | 0.23    |                           |              |       |                           |              |       |                           |              |       |       |        |
| 7   | 0.32  | 16:15:57.14 | -6:03:17.3 | 20.21 | 19.04 | 18.56 | 18.08 | 15.71 | 4.56    | 3.43    | 2.89    | 2.42    | ...                       | ...          | ...   | ...                       | ...          | ...   | ...                       | ...          | ...   | ...   | ...    |
|     | 0.05  |             |            | 0.24  | 0.09  | 0.06  | 0.06  | 0.03  | 0.32    | 0.20    | 0.19    | 0.19    |                           |              |       |                           |              |       |                           |              |       |       |        |
| 8   | 0.19  | 16:15:40.11 | -6:01:04.2 | 20.08 | 19.03 | 18.48 | 17.97 | 15.39 | 5.08    | 3.68    | 3.05    | 2.54    | 21.11                     | 0.095        | 2.62  | 20.63                     | 0.129        | 2.66  | 18.36                     | 0.254        | 4.75  | 0.869 | 42.54  |
|     | 0.04  |             |            | 0.24  | 0.09  | 0.06  | 0.06  | 0.02  | 0.40    | 0.21    | 0.19    | 0.19    |                           |              |       |                           |              |       |                           |              |       |       |        |
| 9   | 0.28  | 16:15:38.83 | -6:04:35.1 | 21.38 | 20.62 | 19.95 | 19.17 | 16.79 | 5.09    | 4.33    | 3.47    | 2.80    | ...                       | ...          | ...   | ...                       | ...          | ...   | ...                       | ...          | ...   | ...   | ...    |
|     | 0.12  |             |            | 0.52  | 0.19  | 0.12  | 0.10  | 0.05  | 0.68    | 0.35    | 0.27    | 0.26    |                           |              |       |                           |              |       |                           |              |       |       |        |
| 10  | 0.19  | 16:15:40.27 | -6:03:20.5 | 20.41 | 19.76 | 19.40 | 19.08 | 17.23 | 3.28    | 2.62    | 2.26    | 1.94    | 21.57                     | 0.016        | 0.96  | 20.90                     | -0.082       | 0.85  | ...                       | ...          | ...   | ...   | ...    |
|     | 0.06  |             |            | 0.27  | 0.13  | 0.09  | 0.10  | 0.06  | 0.40    | 0.29    | 0.27    | 0.27    |                           |              |       |                           |              |       |                           |              |       |       |        |
| 11  | 0.19  | 16:15:40.22 | -6:03:08.0 | 22.25 | 20.61 | 19.92 | 19.42 | 17.09 | 5.46    | 3.58    | 2.91    | 2.38    | ...                       | ...          | ...   | ...                       | ...          | ...   | ...                       | ...          | ...   | ...   | ...    |
|     | 0.08  |             |            | 0.73  | 0.19  | 0.12  | 0.11  | 0.05  | 0.86    | 0.30    | 0.26    | 0.25    |                           |              |       |                           |              |       |                           |              |       |       |        |
| 12  | 0.20  | 16:15:40.80 | -6:00:57.6 | 22.40 | 20.63 | 19.89 | 19.46 | 16.68 | 5.41    | 3.92    | 3.23    | 2.72    | ...                       | ...          | ...   | ...                       | ...          | ...   | ...                       | ...          | ...   | ...   | ...    |
|     | 0.07  |             |            | 0.80  | 0.19  | 0.11  | 0.11  | 0.04  | 0.71    | 0.29    | 0.24    | 0.24    |                           |              |       |                           |              |       |                           |              |       |       |        |
| 13  | 0.28  | 16:15:40.80 | -6:01:07.8 | 22.10 | 20.70 | 20.09 | 19.74 | 17.08 | 4.62    | 3.61    | 2.97    | 2.63    | ...                       | ...          | ...   | ...                       | ...          | ...   | ...                       | ...          | ...   | ...   | ...    |
|     | 0.06  |             |            | 0.76  | 0.20  | 0.13  | 0.13  | 0.06  | 0.64    | 0.33    | 0.28    | 0.28    |                           |              |       |                           |              |       |                           |              |       |       |        |
| 14  | 0.14  | 16:15:40.89 | -6:04:13.6 | 20.42 | 19.58 | 19.31 | 18.65 | 16.99 | 4.35    | 3.20    | 2.72    | 2.15    | 22.01                     | 0.082        | 1.52  | 21.74                     | 0.186        | 1.59  | ...                       | ...          | ...   | ...   | ...    |
|     | 0.10  |             |            | 0.30  | 0.12  | 0.09  | 0.08  | 0.05  | 0.55    | 0.29    | 0.26    | 0.26    |                           |              |       |                           |              |       |                           |              |       |       |        |
| 15  | 0.20  | 16:15:41.00 | -6:02:09.7 | 21.36 | 20.00 | 19.38 | 18.90 | 16.39 | 5.15    | 3.76    | 3.07    | 2.57    | 21.73                     | 0.111        | 4.26  | 21.82                     | 0.264        | 4.54  | 18.02                     | -0.012       | 5.74  | 0.863 | -96.65 |
|     | 0.05  |             |            | 0.47  | 0.14  | 0.09  | 0.09  | 0.04  | 0.57    | 0.26    | 0.23    | 0.22    |                           |              |       |                           |              |       |                           |              |       |       |        |
| 16  | 0.28  | 16:15:41.02 | -6:04:41.2 | 21.17 | 20.04 | 19.52 | 19.03 | 16.54 | 4.66    | 3.57    | 3.03    | 2.53    | ...                       | ...          | ...   | ...                       | ...          | ...   | ...                       | ...          | ...   | ...   | ...    |
|     | 0.07  |             |            | 0.40  | 0.14  | 0.10  | 0.09  | 0.04  | 0.47    | 0.26    | 0.23    | 0.23    |                           |              |       |                           |              |       |                           |              |       |       |        |
| 17  | 0.20  | 16:15:41.08 | -6:00:19.8 | 22.26 | 20.14 | 19.45 | 18.94 | 16.46 | 5.46    | 3.68    | 2.98    | 2.47    | 20.60                     | -0.145       | 4.44  | 20.19                     | -0.116       | 4.16  | 16.99                     | -0.273       | 3.61  | 0.427 | -3.62  |
|     | 0.06  |             |            | 0.77  | 0.15  | 0.09  | 0.09  | 0.04  | 0.67    | 0.26    | 0.23    | 0.22    |                           |              |       |                           |              |       |                           |              |       |       |        |
| 18  | 0.45  | 16:15:41.09 | -6:01:24.1 | 22.52 | 21.20 | 20.23 | 19.64 | 16.91 | 5.55    | 4.30    | 3.32    | 2.74    | ...                       | ...          | ...   | ...                       | ...          | ...   | ...                       | ...          | ...   | ...   | ...    |
|     | 0.06  |             |            | 0.83  | 0.24  | 0.13  | 0.12  | 0.05  | 0.84    | 0.34    | 0.26    | 0.25    |                           |              |       |                           |              |       |                           |              |       |       |        |

Table 2. Photometric catalog of A 2163B

two higher density clumps, to about  $-1.4$  into the outer region, implying that the population of dwarf galaxies is less abundant in the higher density environment. This behaviour of the NIR LF is of particular interest, since the K-band light is less sensitive to recent episodes of star formation and follows, therefore, more closely the (luminous) mass distribution in galaxies. The steepening of the NIR LF at lower densities has also been found by previous works (e.g. Andreon 2001), and can be interpreted as due to an increase of the merging rate or by invoking some mechanisms, such as ram pressure or tidal stripping, which 'destroy' galaxies of smaller size in higher density environments.

The present data-set is employed in paper II in order to perform a detailed analysis of the structural parameters of galaxies in A 2163B, studying the internal colour gradients of galaxies and the correlations between structural parameters, that is the Kormendy relation and the Photometric Plane for the population of spheroids at  $z \sim 0.2$ .

*Acknowledgements.* We are grateful to M. Pannella, who made the observations on April 2002. We also thank I. Lehmann for having carefully read our paper.

## References

- Andreon, S. 2001, ApJ, 547, 623
- Andreon, S., & Pelló, R. 2000, A&A, 353, 479
- Arnaud, M., Elbaz, D., Böhringer, H., Soucail, H., & Mathez, G. 1994, in *New Horizon of X-Ray Astronomy*, ed. F. Makino & T. Ohashi (Tokyo: Universal Academy), 537
- Beers, T.C., Flynn, K., & Gebhardt, K. 1990, AJ, 100, 32
- Bertin, E., & Arnout, S. 1996, A&AS, 117, 393
- Bower, R.G., Lucey, J.R., & Ellis, R.S. 1992, MNRAS, 254, 589
- Bruzual, G.A., & Charlot, S., 1993, ApJ, 405, 538
- Burstein, D., & Heiles, C. 1984, ApJS, 54, 33 (BH84)
- Busarello, G., Merluzzi, P., La Barbera, F., Massarotti, M., & Capaccioli, M. 2002, A&A, 389, 787
- Butcher, H., & Oelmer, A. 1978, ApJ, 219, 18
- Colafrancesco, S., Marchegiani, P., & Palladino, E. 2003, A&A, 397, 27
- de Propris, R., Eisenhardt, P.R., Stanford, S.A., & Dickinson, M. 1998, ApJ, 503, 45
- de Propris, R., & Pritchett, C.J. 1998, AJ, 116, 1118 (dPE98)
- de Propris, R., Stanford, S.A., Eisenhardt, P.R., Dickinson, M., & Elston, R. 1999, AJ, 118, 719 (dPS99)
- Elbaz, D., Arnaud, M., & Böhringer, H. 1995, A&A, 293, 337
- Feretti, L., Fusco-Femiano, R., Giovannini, G., & Govoni, F. 2001, A&A, 373, 106
- Garilli, B., Maccagni, D., & Andreon, S. 1999, A&A, 342, 408
- Huang, J.-S., Thompson, D., Kümmel, M.W., et al. 2001, A&A, 368, 787
- Kochanek, C.S., Pahre, M.A., Falco, E.E., et al. 2001, ApJ, 560, 566

- Kodama, T., Arimoto, N., Barger, A.J., & Aragón-Salamanca, A. 1998, *A&A*, 334, 99 (KAB98)
- Kodama, T., & Bower, R.G. 2001, *MNRAS*, 321, 18
- Kron, R.G. 1980, *ApJS*, 43, 305
- La Barbera, Busarello, G., Merluzzi, P. et al. 2003a, *A&A*, 399, 899
- La Barbera, F., Merluzzi, P., Iovino, A., Busarello, G., Massarotti, M., and Capaccioli, M. 2003b, *A&A*, 399, 899
- Landolt, A.U. 1992, *AJ*, 104, 340
- Markevitch, M., Mushotzky, R., Inoue, H., et al. 1996, *ApJ*, 456, 437
- Massarotti, M., Busarello, G., La Barbera, F., & Merluzzi, P. 2003, *A&A*, 404, 75
- Massarotti, M., Iovino, A., Buzzoni, A. 2001a, *A&A*, 368, 74
- Massarotti, M., Iovino, A., Buzzoni, A., & Valls-Gabaud 2001b, *A&A*, 380, 425
- Mercurio, A., Massarotti, M., Merluzzi, P., Girardi, M., La Barbera, F., and Busarello, G. 2003, *A&A*, in press (astro-ph/0303598)
- Merluzzi, P., La Barbera, F., Massarotti, M., Busarello, G., & Capaccioli, M. 2003, *ApJ*, 589, 147
- Parolin, I., Molinari, E., & Chincarini, G. 2003, *A&A*, in press (astro-ph/0306508)
- Persson, S.E., Murphy, D.C., Krzeminski, W., Roth, M., & Rieke, M.J. 1998, *AJ*, 116, 2475
- Pickles, A.J. 1998, *PASP*, 110, 863
- Pozzetti, L., Bruzual A.G., & Zamorani, G. 1996, *MNRAS*, 281, 953
- Press, W.H., & Schechter, P. 1974, *ApJ*, 187, 425
- Schlegel, D., Finkbeiner, D.P., & Davis, M. 1998, *ApJ*, 500, 525 (SFD98)
- Squires, G., Neumann, D.M., & Kaiser, N. 1997, *ApJ*, 482, 648
- Stanford, S.A., Eisenhardt, P.R.M., & Dickinson, M. 1998, *ApJ*, 492, 461
- Trentham, N.D. 1997, *MNRAS*, 294, 193
- Visvanathan, N., & Sandage, A. 1977, *ApJ*, 216, 21
- Worthey, G., Trager, S.C., & Faber, S.M., 1996, in *ASP Conf. Ser. 86, Fresh Views of Elliptical Galaxies*, ed. A. Buzzoni, A. Renzini, & A. Serrano (San Francisco: ASP), 203